

See discussions, stats, and author profiles for this publication at: <https://www.researchgate.net/publication/255245769>

Modeling the Interaction between Integrin-Binding Peptide (RGD) and Rutile Surface: The Effect of Na⁺ on Peptide Adsorption

ARTICLE in THE JOURNAL OF PHYSICAL CHEMISTRY C · NOVEMBER 2011

Impact Factor: 4.77 · DOI: 10.1021/jp2061915

CITATIONS

11

READS

37

5 AUTHORS, INCLUDING:



Chunya Wu

Harbin Institute of Technology

12 PUBLICATIONS 101 CITATIONS

[SEE PROFILE](#)



Adam Arnold Skelton

University of KwaZulu-Natal

27 PUBLICATIONS 267 CITATIONS

[SEE PROFILE](#)



Lukas Vlcek

Oak Ridge National Laboratory

67 PUBLICATIONS 682 CITATIONS

[SEE PROFILE](#)



Peter T Cummings

Vanderbilt University

518 PUBLICATIONS 11,681 CITATIONS

[SEE PROFILE](#)

Modeling the Interaction between Integrin-Binding Peptide (RGD) and Rutile Surface: The Effect of Na^+ on Peptide Adsorption

Chunya Wu,^{*,†,‡} Adam A. Skelton,^{‡,§} Mingjun Chen,[†] Lukas Vlček,[§] and Peter T. Cummings^{‡,||}

[†]Center for Precision Engineering, Harbin Institute of Technology, P.O. Box 413, Harbin 150001, China

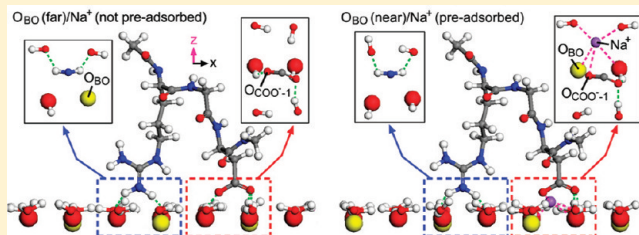
[‡]Department of Chemical & Biomolecular Engineering, Vanderbilt University, Nashville, Tennessee 37235-1604, United States

[§]Chemical Sciences Division and ^{||}Center for Nanophase Materials Sciences, Oak Ridge National Laboratory, Oak Ridge, Tennessee 37831-6494, United States

Supporting Information

ABSTRACT: The dynamics of a single tripeptide Arg-Gly-Asp (RGD) adsorbing onto negatively charged hydroxylated rutile (110) surface in aqueous solution was studied using molecular dynamics (MD) simulations. The results indicate that the adsorbed Na^+ ions play an important role in determining the binding geometry of RGD. With an initial “horseshoe” configuration, the charged side groups (COO^- and NH_2) of the peptide are able to interact with the surface through direct hydrogen bonds (H bonds) in the very early stage of adsorption.

The Na^+ ions approach the positively charged Arg side chain, competing with the Arg side chain for adsorption to the negatively charged hydroxyl oxygen. In coordination with the structural adjustment of the peptide, the Arg residue is driven to detach from the rutile surface. In contrast, the Na^+ ions in close proximity to the negatively charged Asp side chain contribute to the binding of the COO^- group on the surface, helping the carboxyl oxygen not involved in COO^- -surface H bonds to orientate toward the hydroxyl hydrogens. Once both carboxyl oxygens form enough H bonds with the hydroxyl hydrogens, the redundant ions move toward a more favorable adsorption site.



INTRODUCTION

Interfacial interactions between proteins and biomaterials play a vital role in determining cellular responses to foreign implants.^{1–6} When a surface is exposed to a multicomponent solution (e.g., body fluids), proteins will be preferentially deposited from the bulk, saturating the surface within a time frame of seconds to minutes.⁷ The living cells approaching later interact with the adsorbed protein layer rather than the surface itself, enabling the cell membrane-bound receptors to search for the bioactive sites with binding specificity.⁸ The key to controlling cellular response is to manage the type and state of bioactive site presented by the adsorbed protein.⁸ Artificially incorporating bioadhesive motifs with specific recognition properties to the surface of the biomaterial (precoating, *in vitro*) may be a very promising approach to endow the implant with the required biocompatibility. This engineered biomimetic approach may open up new avenues for the design and utilization of biomolecule–material interfacial systems in a wide-range of applications from tissue engineering to various areas of nanotechnology.^{9,10}

The precoating bioadhesive protein layer must withstand competitive adsorption from the soluble proteins in serum, which will interact with the surface of the implant, even if it has already been occupied,^{11,12} as well as the combined effect of water, ions, and surface characteristics, which can determine whether the protein–surface interaction is enhanced or hindered.¹³ The importance

of interfacial water layers in mediating protein adsorption to rutile has been previously addressed.^{14,15} Furthermore, experimental^{16–20} and theoretical^{21–24} studies have been devoted to the influence of material properties (e.g., hydrophilicity, surface topography, and surface charge) on protein adsorption. The Arg-Gly-Asp sequence (RGD, a ubiquitous adhesive motif in extracellular matrix proteins), which has a high affinity to the predominant osteoblast integrin,^{25,26} is regarded to be one of the best candidates for biomimic coating of bone-anchored implants.^{27,28} Despite its importance, only a few simulation studies have been devoted to investigating the adsorption of RGD tripeptide on titanium oxide surfaces.^{21,24,29} Schneider and Ciacchi²⁹ found that the adsorption of solvated RGD on the oxidized Ti(0001) surface was considerably stronger and might thus limit the functionality of the sequence using a classical potential. The MD calculations performed by Zhang et al.²⁴ revealed a complicated step-edge effect on peptide adsorption. The interaction between RGD and the TiO_2 substrate would be weakened when RGD was on the top of the step edge; however, the interaction would be strengthened when RGD fell into the nanoscale grooves formed by step edges. In Chen's²¹ previous MD

Received: June 30, 2011

Revised: October 2, 2011

Published: October 10, 2011

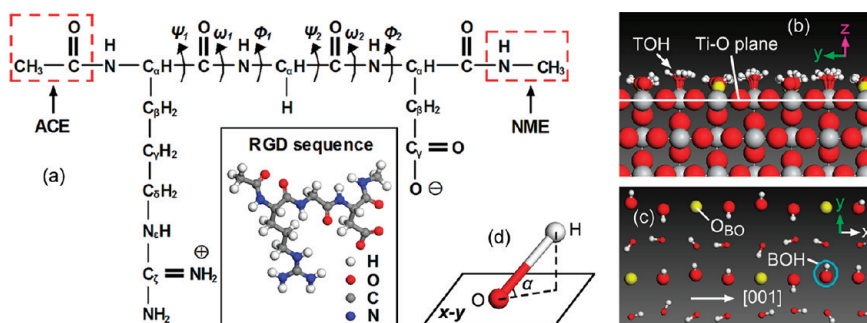


Figure 1. (a) Structure of RGD tripeptide, (b) the structure of the hydroxylated rutile TiO_2 (110) surface, (c) the distribution of the deprotonated sites (O_{BOH} , highlighted in yellow) with respect to the other protonated sites (TOH and BOH), and (d) the geometric scheme of angle α between the $\text{O}_{\text{OH}}-\text{H}_{\text{OH}}$ bond and the $x-y$ plane. The ACE and NME blocking groups are labeled by dashed rectangles.

simulation work, RGD bound to the reduced nonhydroxylated rutile (110) surface (some atoms in the top layer were removed to produce a rectangular groove) exhibited a higher adsorption energy than that on the ideal flat surface. These results revealed some interesting aspects of RGD adsorption on the Ti oxide layer; however, the hydroxylation state and the charge of TiO_2 surface were not involved, which should be important in determining the binding properties of RGD on the surface and will be considered in the present work.

Under physiological conditions, the negative charge of the TiO_2 surface will be screened by counterions beyond $\sim 10 \text{ \AA}$.² If a negatively charged protein is within 10 \AA from the surface, specific intermolecular interactions dominate and gross electrostatic repulsion is not a significant factor.² Many researchers have investigated the effect of salt concentration on protein adsorption using experimental approaches.^{30–35} When exploring the effect of electrostatic attraction/repulsion, it is important to consider the isoelectric point (pI) of both the surface and the protein. At a pH below their pI, the surface and the protein carry a net positive charge (\oplus); above their pI, they carry a net negative charge (\ominus). Topoglidis et al.³⁰ found that increased salt concentration in sodium phosphate buffer (pH 7) led to a weakened binding between cytochrome *c* (\oplus) and the anatase TiO_2 (\ominus) and to a higher level of protein desorption from the surface after full adsorption, attributed to the increased charge screening of the TiO_2 surface by sodium ions. Jonsson et al.^{31,32} observed a small increase in L-aspartate and L-glutamate adsorption on rutile surface with decreasing ionic strength at $3 < \text{pH} < 5$ (rutile: \oplus ; 50% of aqueous L-aspartate: \ominus ; 40% of aqueous L-glutamate: \ominus), but opposite trends were presented at $\text{pH} > 6.5$ when both the adsorbate and the adsorbent were negatively charged. Sano and Shiba³³ stated that the binding of the 12-mer peptide SYRLPVYLLHALL (\ominus) on the Ti-surface (\ominus) was increased at the higher NaCl concentration (500 vs 150 mM), but the binding of RKLDPAPGMHTW (\ominus) was unaffected by increases in the ionic strength of the buffer (pH 7.5). Hayashi et al.^{34,35} used atomic force microscopy and found that the long-range interactions between the Ti-surface and the peptide in the N-terminal domain of ferritins were diminished at high ionic concentrations, but the adhesion forces did not appear to depend on the ionic concentration. The discrepancy existing in these experiments motivates us to investigate how ions mediate and regulate the adsorption activity of protein on inorganic surface at the molecular level.

MD simulations were carried out in the present study to describe the early adsorption process of a single tripeptide RGD

onto the hydroxylated rutile (110) surface at $\text{pH} \sim 7.80$, where Arg and Asp carry a positive and negative charge, respectively. The pI of rutile is ~ 5.30 at 35°C ,³⁶ and thus a negative surface-deprotonation-induced charge (charge density: $\sigma = -0.208 \text{ C/m}^2$)³⁷ is developed at $\text{pH} \sim 7.80$. A strong electrostatic attraction between the positively charged Arg residue and the negatively charged surface is expected,^{33,38–40} whereas an electrostatic repulsion should exist between the Asp and the surface at $\text{pH} \sim 7.80$, where both carry a net negative charge.^{31,32,41–43} Therefore, in this work, we investigated how the presence of Na^+ ions in the vicinity of the charged residues would affect the electrostatic repulsion/atraction and, therefore, the binding propensities of RGD to the negatively charged hydroxylated rutile (110) surface.

SIMULATION METHODOLOGY

Figure 1a gives the structure of the RGD sequence at the desired pH in our simulations ($\text{pH} \sim 7.80$). The side chain of Arg ($\text{pK}_a = 12.0$) was protonated and carried a net positive charge, whereas the side chain of Asp ($\text{pK}_a = 3.90$) was deprotonated and thus carried a negative charge. The blocking group ACE was added to the N-terminus of the RGD, and the blocking group NME was added to the C-terminus to supply a peptide bond as would appear in the protein. The elementary structure of the fully hydroxylated rutile cell with bridging (BOH, formed by adding a hydrogen atom to the bridging oxygen) and terminal hydroxyls (TOH, the hydroxyl groups bind to the terminal five-fold coordinated surface Ti atoms) was obtained from ab initio calculations, as presented in a previous published work.⁴⁴ This unit cell ($l_x = 5.918 \text{ \AA}$, $l_y = 6.497 \text{ \AA}$) was replicated eight times in both x and y directions, and an MD simulation box with the size roughly equal to $47.34 \times 51.98 \times 50 \text{ \AA}^3$ was created.

We carried out MD simulations of the RGD/rutile/aqueous solution system in the NVT ensemble using the program package LAMMPS.⁴⁵ The system was modeled adopting the AMBER force field⁴⁶ for the peptide and the force field reported by Bandura et al.^{37,47,48} for the rutile surface. Periodic boundary conditions were applied in the x and y directions, and reflecting boundary condition was applied in the z direction. The Nosé–Hoover thermostat⁴⁹ was utilized to control the temperature with a time step of 2 fs. Ewald summation was employed to handle the long-range electrostatic interactions with a cutoff distance of 12 \AA . In our simulations, all atoms on and below the surface $\text{Ti}-\text{O}$ plane (shown as large spheres in Figure 1b) were held rigid, whereas the surface atoms above the $\text{Ti}-\text{O}$ plane were kept flexible within fixed lengths of $\text{Ti}-\text{O}$ bonds

Table 1. Charges of Surface Atoms for the Negatively Charged Hydroxylated Rutile (110) Surface

atom	charge	atom	charge
TiT	2.134	TiB	2.134
O _{TOH}	-0.960	O _{BOH}	-0.985
H _{TOH}	0.409	H _{BOH}	0.434
O _{3-fold} ^a	-1.098	O _{BO}	-1.039
Ti _{bulk} ^b	2.196	O _{bulk} ^c	-1.098

^a Three-fold coordinated oxygen on the Ti—O plane. ^b Bulk titanium. ^c Bulk oxygen.

(only for the terminal oxygen (O_{TOH}) and the deprotonated bridging oxygen (O_{BO})) and O—H bonds (for the surface hydroxyl groups). The solvent (water and Na^+ , Cl^- ions) in the molecular assembly was allowed to move for 50 ps at 310.15 K to randomize its position, whereas the peptide was fixed in its spatial location with the original conformation. After an energy minimization (corresponding to approximate 0 K), the RGD was released, and the system temperature was increased gradually in steps of 50 K from 0 to 300 K.¹⁴ The molecular assembly was equilibrated for 40 ps at each intermediate temperature, before commencing on the production run at 310.15 K.

To generate the initial configurations for our runs of RGD on the negatively charged hydroxylated surfaces, we first put RGD close to the neutral hydroxylated rutile (110) surface (i.e., fully hydroxylated surface), with six different starting arrangements obtained by rotating the peptide in $\sim 60^\circ$ increments around the [001] direction (indicated in Figure 1c), as reported in a previous work.⁵⁰ The equilibration course was used as outlined above, and the production run typically lasted for 2 ns. A configuration reminiscent of the “horseshoe” structure^{14,33} with both Arg and Asp side chains attached to the surface was intermittently observed in the simulations. We chose a “horseshoe” configuration from the molecular assembly, which presented the minimal energy of the simulation system and took this configuration as the initial state of RGD on the desired surface. The negatively charged rutile introduced here is a surface with a full coverage of TOH and a smaller coverage of BOH (25% of the BOH groups were deprotonated to create the surface charge: $\sigma = -0.208 \text{ C/m}^2$).³⁷ Table 1 lists the partial charges of surface atoms, and Figure 1c displays the distribution of the deprotonated sites (O_{BO} , highlighted in yellow) with respect to the other protonated sites (TOH and BOH), in a pattern that allows maximum separation of like-charged groups.

To find out the effects of surface deprotonation and ion mediation on RGD/rutile binding propensity, we established three different simulation systems. (The starting conformations are shown in Figure 2.) System I was designed to test the influence of partial deprotonation of surface sites on the adsorption mode of RGD when the Arg (inset in Figure 2a, left) and Asp side chains (inset in Figure 2a, right) were initially H-bonded to the surface hydroxyls. Moreover, it was also interesting to find out whether the ions could approach the adsorption sites to strengthen/weaken RGD/rutile binding further. Hence, in system I (Figure 2a), 32 bridging hydroxyl hydrogens (H_{BOH}) were removed to create the negative charge of the surface, but none of these H_{BOH} atoms was originally in close proximity (directly H-bonded) to the oxygens in the Asp γ -carboxyl (O_{COO^-}). All ions were positioned far away from the Ti—O plane ($> 8 \text{ \AA}$). Hereafter we called system I “ O_{BO} (far)/ Na^+ (not preadsorbed)”.

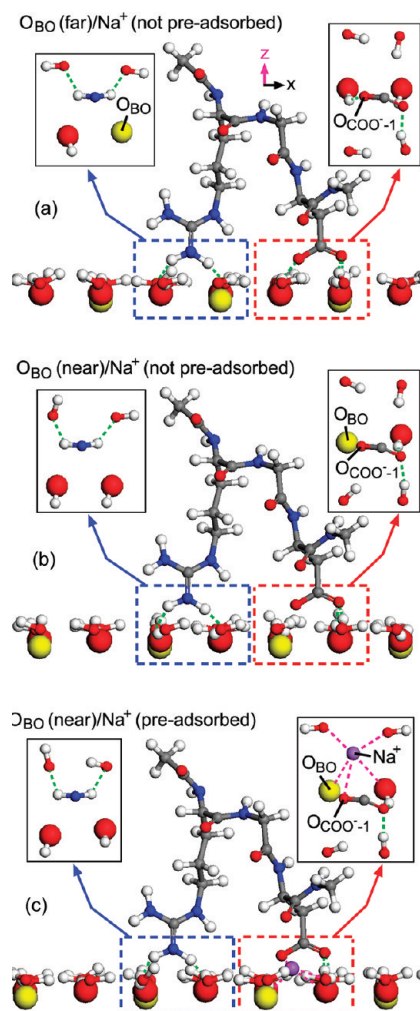


Figure 2. Initial configurations of three simulation systems: (a) system I: O_{BO} (far)/ Na^+ (not preadsorbed), (b) system II: O_{BO} (near)/ Na^+ (not preadsorbed), and (c) system III: O_{BO} (near)/ Na^+ (preadsorbed). The insets show the NH_2 -surface binding site (left) and the COO^- -surface binding site (right). Part of the surface groups are omitted for clarity. The O_{BOH} and O_{BO} (highlighted in yellow) are shown by CPK mode (large spheres), and the H_{BOH} , TOH, RGD atoms and the Na^+ ions are shown by ball-and-stick mode. The H bonds and direct bonds (connected to the Na^+ ions) are represented by green and magenta dashed lines, respectively.

System II (“ O_{BO} (near)/ Na^+ (not preadsorbed)”) was used to understand the nature of adsorption of the negatively charged Asp side chain on the deprotonated part of the rutile (110) surface without the involvement of cations, that is, whether the Asp side chain can remain attached to the surface when the H_{BOH} closest to the O_{COO^-} was taken away. The initial state of system II (e.g., the spatial positions of RGD, ions, etc.) was identical to the one of system I, except for a different distribution of O_{BO} atoms (yellow spheres). As shown in Figure 2b, the O_{COO^-} atom was close to a deprotonated O_{BO} atom, and no H_{BOH} was available to form a H bond; however, the H bonds between the other O_{COO^-} and the surface hydrogens were kept. System III was established to see how the Asp/rutile binding in system II would change when there was a cation close enough to possibly mediate the Asp-surface interaction. Because system III was similar to system II, except that a Na^+ ion was initially positioned

in the vicinity of O_{COO^-} atoms (inset in Figure 2c, right), it was called “ O_{BO} (near)/ Na^+ (preadsorbed)”. The RGD-TiO₂ complexes in the three systems were immersed in 2194 SPC/E water molecules. To ensure the overall charge neutrality of the simulation system, 48 Na^+ ions and 16 Cl^- ions were added in the solvent to compensate the total negative charge of $-32e$ in the surface. A 6 ns production simulation was performed for each molecular assembly with snapshots taken every 3 ps.

RESULTS AND DISCUSSION

Skelton et al.¹⁴ found that the RKL PDA peptide might initially recognize the interfacial water layers and interact with the non-hydroxylated rutile surface via these water layers (in a “horse-shoe” configuration). This emphasizes the necessity to analyze the binding geometries of water molecules in contact with the surface hydroxyls on the rutile (110). The behavior of Na^+ ions at the rutile/water interface will also be discussed to help to evaluate the effect of adsorbed compensating Na^+ on the binding of RGD to the negatively charged hydroxylated rutile (110) surface. However, the role of Cl^- ions in RGD adsorption will not be mentioned in detail because the anions cannot directly adsorb or approach closely to the negatively charged surface, thereby having little impact on the peptide binding. This accords with Köppen’s MD results⁵¹ that ions with the same sign of charge as the surface tended to diffuse into the bulk, even initially concentrated close to the surface. The distributions of water and cations with respect to the surface were almost identical in the three simulations because the equilibration time was long enough to allow the cations to drift from the initial positions toward the surface. Hence, system I was selected for a detailed analysis of the interfacial interactions between the water, Na^+ ions and the surface hydroxyls. The dynamics of RGD in the three simulation systems will be analyzed separately. O_w , O_{TOH} , and O_{BOH} refer to oxygens in the water, TOH group, and BOH group, respectively, and H_w , H_{TOH} , and H_{BOH} refer to hydrogens in the water, TOH group, and BOH group, respectively. O_{OH} and H_{OH} are the generic term for all hydroxyl oxygens (O_{TOH} and O_{BOH}) and hydroxyl hydrogens (H_{TOH} and H_{BOH}), respectively. Bridging oxygen is the generic term for O_{BO} and O_{BOH} . Ti_T and Ti_B refer to surface titaniums bound to O_{TOH} and bridging oxygens, respectively.

General Aspects of the Water–Surface Interaction. Water molecules are adsorbed on the hydrophilic rutile surface through a network of H bonds.⁵² To give a reasonable description of the interactions between the adsorbate and the adsorbent, H bonds were counted when the donor···acceptor distance was $<3.4 \text{ \AA}$, and the donor-H···acceptor angle was $>135^\circ$ (e.g., for two water molecules, this criterion corresponds to the $O_w \cdots O_w$ distance $<3.4 \text{ \AA}$ and the $O_w - H_w \cdots O_w$ angle $>135^\circ$). Similar definitions have been used by other authors.^{53–55} When a water molecule approaches the TOH or BOH group, two kinds of H bonds, that is, the $H_w \cdots O_{OH}$ H bond and the $H_{OH} \cdots O_w$ H bond, can be created. (The oxygen linked to the hydrogen by “···” is the H-bond acceptor.)

Figure S1 in the Supporting Information shows the available binding modes of a single TOH or BOH group with the H-bonded water molecules as well as the percentage of each mode (per hydroxyl). When waters approach, a single TOH group is capable of forming a maximum of three H bonds with the surrounding waters, whereas a maximum of two H bonds can exist between a single BOH group and the approaching waters. Table 2 lists the statistical parameters of H bonds between a

Table 2. Parameters of Water-TOH, BOH, and O_{BO} H Bonds

items	TOH	BOH	O_{BO}
$n_{HB\text{-water}}^b$	0.73	0.57	0.82
$n_{HB}(H_w \cdots O_{OH} \text{ H bond})$	0.56	0.34	0.82
$n_{HB}(H_{OH} \cdots O_w \text{ H bond})$	0.17	0.23	
$l_{HB}(H_w \cdots O_{OH}) (\text{\AA})^c$	1.83	1.89	1.73
$l_{HB}(H_{OH} \cdots O_w) (\text{\AA})^c$	2.11	2.02	

^a Items represented by O_{OH} apply to the ones for O_{BO} . ^b Average number of H-bonded water molecules per hydroxyl or O_{BO} . ^c Distance between the hydrogen and the H-bond acceptor.

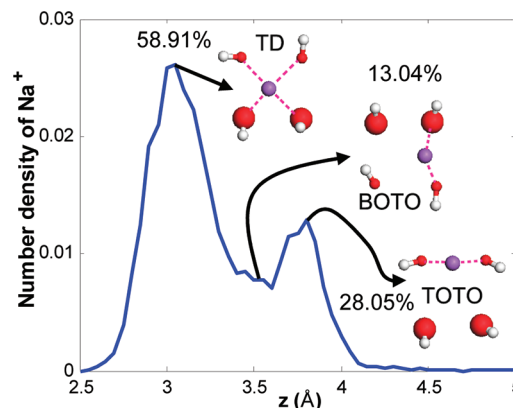


Figure 3. Axial density profile of Na^+ ions in system I. The numbers positioned close to the snapshots are the percentages of adsorbed Na^+ at the specific adsorption sites relative to the total number of Na^+ ions in the region, 0–5 Å from the surface.

single surface hydroxyl (including O_{BO}) and the surrounding waters. The TOH group interacts more actively with the water than the BOH group, inferred from the total number of H-bonded waters per hydroxyl (0.73 vs 0.57). For a single TOH group, the number of $H_w \cdots O_{OH}$ H bonds is more than three times as large as the number of $H_{OH} \cdots O_w$ H bonds. However, the $H_w \cdots O_{OH}$ and $H_{OH} \cdots O_w$ H bonds for a single BOH are comparable in number. The $H \cdots$ acceptor distance in $H_w \cdots O_{OH}$ H bond for the TOH group (1.83 Å) is smaller than the equivalent value for the BOH group (1.89 Å), but the $H \cdots$ acceptor distance in $H_{OH} \cdots O_w$ H bond for the former (2.11 Å) is much larger than the latter (2.02 Å). It may be inferred by the differences in H-bond numbers that the accessibility of H_w to the O_{TOH} is greater than H_w to the O_{BOH} , whereas the accessibility of O_w to the H_{TOH} is less than O_w to the H_{BOH} . The differences in H-bond lengths indicate that the $H_w \cdots O_{TOH}$ H bond is stronger than the $H_w \cdots O_{BOH}$ H bond, whereas the $H_{TOH} \cdots O_w$ H bond is weaker than the $H_{BOH} \cdots O_w$ H bond. These can be explained by the angle α between the $O_{OH}-H_{OH}$ bond and the $x-y$ plane (illustrated in Figure 1d). Angle α for the TOH group ($\alpha = 19.12^\circ$) is much smaller than the one for the BOH group ($\alpha = 32.02^\circ$), providing a greater exposure of the O_{TOH} to the H_w . Moreover, a smaller angle α orients the H_{TOH} toward the $x-y$ plane (i.e., a nearly parallel $O_{TOH}-H_{TOH}$ bond with respect to the $x-y$ plane), making it difficult to be pulled into the solvent to form the $H_{OH} \cdots O_w$ H bond.

In summary, H_w atoms are more attracted to the O_{TOH} than the O_{BOH} , whereas O_w atoms are more attracted to the H_{BOH} than the H_{TOH} . On the basis of these findings, we can now ask the

Table 3. Parameters of the Adsorbed Na⁺ on a Single Surface Group

items	TOH	BOH	BO
number of adsorbed Na ⁺	0.60	0.43	0.51
length of Na ⁺ –O bond (Å)	2.51	2.71	2.72

following questions: Does the fact that there is a strong H bond to the respective hydroxyl groups suggest an inherent nature to the H bonds to these groups? That is, will the fact that there is a strong H bond between O_{TOH} and H_w mean that there will also be strong H bonds between O_{TOH} and the positively charged NH₂ groups of Arg? Moreover, will the fact that there is a strong H bond between H_{BOH} and O_w mean that there will be strong H bonds between H_{BOH} and the negatively charged COO[−] group of Asp?

General Behavior of Na⁺ at the Rutile/Water Interface. It will be shown that Na⁺–surface interactions play an important role in determining the binding mode of RGD. Therefore, the adsorption sites of cations on the negatively charged hydroxylated rutile (110) surface should be examined. The criterion of Na⁺–O interaction, also adopted by Předota et al.,⁵⁶ is explained in Figure S2 in the Supporting Information. Figure 3 shows the axial density profile of Na⁺ (the number of ions per cubic angstrom), in which the zero point of horizontal axis was defined as the position that the surface layer of Ti atoms would occupy in the unrelaxed crystal termination. The Na⁺ ions adsorb on the surface at three different kinds of adsorption sites, which are displayed in the snapshots in Figure 3. The numbers positioned close to the snapshots are the percentages of the adsorbed Na⁺ at different adsorption sites relative to the total number of cations in the region of 0–5 Å from the surface. The first peak in the axial density refers to the Na⁺ ions adsorbing at a tetradeinate site (TD) with an average height of 3.04 Å. The predominance of the TD Na⁺ may imply a more stable configuration, which is probably the most important adsorption mode of Na⁺ for mediating peptide/surface binding. The small shoulder of the axial density profile at ~3.49 Å is formed by a minority of bidentate Na⁺ ions (BD-BOTO), which bind to one O_{TOH} and one bridging oxygen. Na⁺ ions adsorbing at a more popular bidentate site (BD-TOTO, at a height of ~3.78 Å) form interactions with two O_{TOH} atoms.

The H_{OH} atoms minimize the Na⁺–H repulsions by moving away from the Na⁺ ions (snapshots in Figure 3). However, the frozen surface Ti atoms connected with the O_{OH} or O_{BO} are unable to move. Therefore, Na⁺–Ti repulsions are inevitable when the cations reach the surface and form Na⁺–O bonds. This is especially the case for the Na⁺ approaching the bridging oxygen, which is coordinated to two adjacent Ti_B atoms. However, the adsorbed Na⁺ may be capable of orientating itself toward a favorable position to minimize the Na⁺–Ti repulsion. We speculate that the adsorbed Na⁺ may be pushed a bit farther away from the O_{BO} or O_{BOH} than the O_{TOH} (only connected to one Ti_T atom) due to the combined effect of Na⁺–Ti repulsion and Na⁺–O attraction. Table 3 lists the average number of Na⁺ ions interacting with a single O_{TOH}, O_{BOH}, or O_{BO} as well as the lengths of Na⁺–O bonds. As mentioned in the last section, a smaller angle α for the TOH group also provides a greater exposure of the O_{TOH} to the Na⁺ than the O_{BOH}, confirmed by the number of adsorbed Na⁺ per O_{OH} (O_{TOH}: 0.60 vs O_{BOH}: 0.43). However, the number of Na⁺ adsorbed on the O_{BO} is a

little smaller than the one on the O_{TOH}. This probably results from a larger number of H-bonded water molecules with shorter H_w···acceptor distances on the O_{BO} (Table 2, TOH: $n_{\text{HB-water}} = 0.73$, $l_{\text{HB}}(\text{H}_w \cdots \text{O}_{\text{TOH}}) = 1.83$ Å; O_{BO}: $n_{\text{HB-water}} = 0.82$, $l_{\text{HB}}(\text{H}_w \cdots \text{O}_{\text{BO}}) = 1.73$ Å), which will compete with the Na⁺ ions for adsorption to the O_{BO}. Therefore, a longer Na⁺–O_{BO} bond (2.72 Å) may be attributed to the combined effect of stronger Ti repulsion and greater water competition. A much shorter Na⁺–O bond for the TOH group (2.51 Å) further confirms the assumption about the contribution of the repulsion from the surface Ti in Na⁺ adsorption (i.e., the repulsion from one Ti_T is weaker than that from two Ti_B). This may be also the reason for the absence of the BD-BOBO adsorption site for Na⁺. The H_{OH}–Ti repulsions work in a similar way as the Na⁺–Ti repulsions because both H_{OH} and the adsorbed Na⁺ are positively charged and close to the O_{OH}. Therefore, it can be inferred that a smaller angle α for the TOH group, that is, a nearly parallel O_{TOH}–H_{TOH} bond with respect to the x – y plane, may be partially derived from a weaker H_{TOH}–Ti_T repulsion. Additionally, the stronger H_{BOH}–Ti_B repulsion may push the H_{BOH} toward the solvent, which leads to a larger angle α and thus less accessibility of H_w to the O_{BOH}. The results so far have shown that both H_w atoms and Na⁺ ions prefer the O_{TOH} to the O_{BOH}.

RGD–Surface Interaction. During the production runs of the three simulations, the distances from the NH₂ groups to the nearest O_{TOH} are shorter than the distances to the nearest O_{BOH} and O_{BO} (Figure S3 in the Supporting Information). The distances from the COO[−] group to the nearest surface hydrogens (H_{TOH} and H_{BOH}) show that sometimes the O_{COO[−]} can form H bonds with both H_{TOH} and H_{BOH}, but the distance from the O_{COO[−]} to the H_{BOH} is much shorter than the one to the H_{TOH} (Figure S4 in the Supporting Information). That is, the distances from NH₂, COO[−] groups to the surface hydroxyls show a similar trend to the water–hydroxyl interaction. Hence we may infer here that the O_{TOH} shows a stronger attraction for the positively charged species (H_w, Na⁺, and NH₂) than the O_{BOH}, whereas the H_{BOH} is more attracted to the negatively charged species (O_w and COO[−]) than the H_{TOH}.

When considering how the peptide interacts with the surface, the distance from Asp and Arg to the surface should be crucial. The peptide–surface distances for each simulation system are shown in Figure 4 (system I: (a); system II: (b); system III: (c)). The NH₂-1 group in system I (O_{BO} (far)/Na⁺ (not pre-adsorbed)) remains close to the surface ($d_{\text{N}-\text{O}} = 3.05$ Å) in the early stage of the production run ($t < 1.80$ ns), facing its two hydrogens toward the rutile surface (Figure 4a-(1)). With the approach of Na⁺ and the structural adjustment of the peptide (see below), the Arg side chain gradually comes off the surface after 2.30 ns. The COO[−] group in system I coordinates to the H_{BOH} atoms stably ($d_{\text{O}-\text{H}} = 1.49$ Å, $\sigma=0.14$ Å) during the entire simulation, except when one of the H_{BOH}···O_{COO[−]} H bonds occasionally breaks. Furthermore, the mediated Na⁺ at a TD site acts as a bridge between the O_{COO[−]} atoms and the surface (Figure 4a-(2)), helping to stabilize the Asp. In contrast, the H_{BOH} that previously forms a H bond with O_{COO[−]-1} is removed in system II (O_{BO} (near)/Na⁺ (not pre-adsorbed)). The COO[−] group with one O_{COO[−]} attached to the surface and the other free (Figure 4b-(1)) leaves the surface before the Na⁺ arrives in the vicinity of the Asp side chain to mediate the Asp–surface interaction. The Arg side chain stays close to the O_{TOH} ($d_{\text{N}-\text{O}} = 3.08$ Å) for ~4.60 ns (Figure 4b-(2)) but is driven away from the surface by the repulsion from the nearby Na⁺ ions (see below).

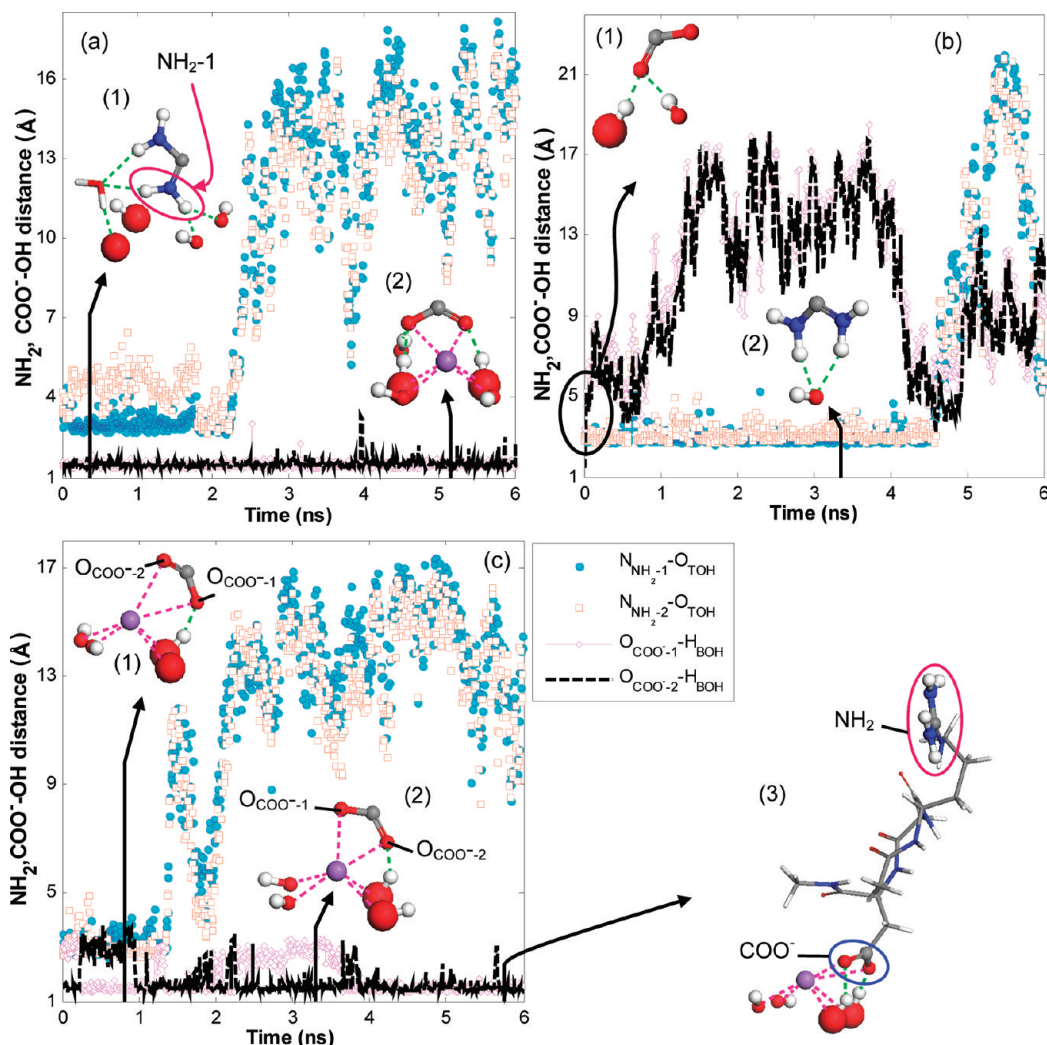


Figure 4. Evolution of the distances from the NH₂ and COO⁻ groups to the nearest surface hydroxyls during the 6 ns MD production run. (a) System I, (b) system II, and (c) system III. O_{TOH} refers to oxygens in the TOH groups, H_{BOH} refers to hydrogens in the BOH groups. In the snapshot, the O_{BOH} and O_{BO} are shown by CPK mode, and the H_{BOH}, TOH, COO⁻, NH₂, and the adsorbed Na⁺ ions are shown by ball-and-stick mode. The H bonds and direct bonds (connected to the Na⁺ ions) are represented by green and magenta dashed lines, respectively.

In system III (O_{BO} (near)/Na⁺ (predisorbed)), the Arg is close to the surface ($d_{N-O} = 3.09 \text{ \AA}$) at the beginning of the simulation but starts to leave the surface at $t = 1.40 \text{ ns}$. The Arg, however, returns at $t = 2 \text{ ns}$, then detaches from the surface completely after only 0.40 ns. That is, the Arg undergoes a sudden “leave-return-leave” motion before full desorption. The predominant conformation of the COO⁻ group before 4 ns is one where one O_{COO-} coordinates to both the H_{BOH} and the predisorbed Na⁺, whereas the other O_{COO-} not involved in H bonds with the surface forms bonds with the nearby Na⁺ (Figure 4c-(1), (2)). After 4 ns, both O_{COO-} atoms form H bonds with the neighboring H_{BOH} and usually form direct bonds with the mediated Na⁺ (Figure 4c-(3)), similar to the binding mode of COO⁻ in system I (Figure 4a-(2)). That is, the RGD in both systems I and III finally undergoes the “hinge-bending” motion,⁵⁷ where one end of the molecule (COO⁻) is attached to the surface and the other end (NH₂) is free to move in the solvent phase (Figure 4c-(3)).

Overall, approaching Na⁺ ions compete with the NH₂ for the adsorption site. The flexible side chain of Arg exhibits some rotational freedom and lateral mobility, causing it to move away from the Na⁺ ions. However, the Arg residue finally leaves the

surface completely, due to the combined effect of structural adjustment and Na⁺ repulsion. On the contrary, if the COO⁻ group can remain on the surface for a certain time, which is long enough to allow the Na⁺ ions to reach the negatively charged rutile (110) surface, then the adsorbed Na⁺ ion in close proximity to the Asp side chain seems to provide a strong bridge to link the COO⁻ and the rutile surface. On the basis of the general results presented above, we studied the simulation results in detail to gain some insight into the contribution of the adsorbed compensating Na⁺ ions to the adsorption of negatively charged COO⁻ group and the desorption of positively charged NH₂ group.

Effect of Na⁺ on Asp Adsorption. The role of cations in the adsorption of negatively charged proteins on the negatively charged surfaces has been highlighted in experimental studies.^{30–33} Therefore, it would be interesting to analyze how the Na⁺ ions mediate and facilitate the adsorption of negatively charged Asp on the negatively charged rutile (110) surface. The 2D density maps within the region $16 \leq x \leq 32$, $15 \leq y \leq 30$ for systems I and III during the final 2 ns of simulation are displayed in Figure 5 to visualize the positions of the adsorbed Na⁺ and the COO⁻

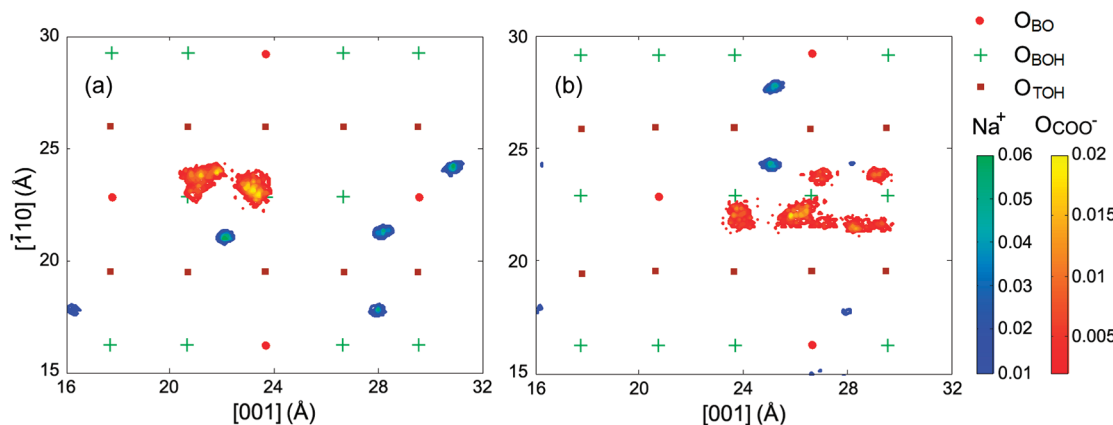


Figure 5. Two-dimensional density maps of the adsorbed Na^+ ions and the COO^- group on the negatively charged rutile (110) surface during the final 2 ns simulation time: (a) system I and (b) system III. Color codes: O_{BO} , red dot; O_{BOH} , green plus; O_{TOH} , brown square.

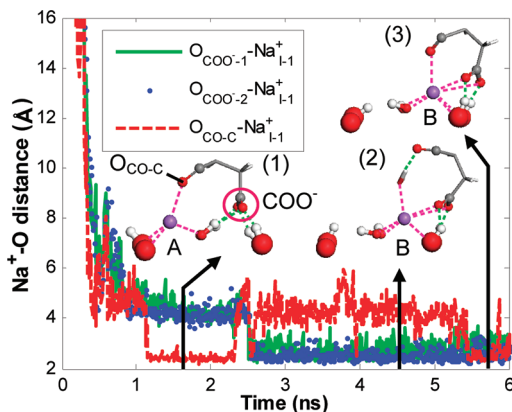


Figure 6. Evolution of the distances from the $\text{O}_{\text{COO}-}$ and $\text{O}_{\text{CO}-\text{C}}$ (carbonyl oxygen in the C-terminus) to the $\text{Na}^+_{\text{I}-1}$ ion for system I during the 6 ns MD production run. In the snapshots, the O_{BOH} and O_{BO} are shown by CPK mode, the H_{BOH} , TOH , COO^- , CO , and the adsorbed Na^+ ions are shown by ball-and-stick mode; the involved water molecule is shown by stick mode. The H bonds and direct bonds (connected to the Na^+ ions) are represented by green and magenta dashed lines, respectively.

group on the surface. When both $\text{O}_{\text{COO}-}$ atoms initially coordinate to the hydroxylated surface through an adequate number of H bonds (e.g., system I: O_{BO} (far)/ Na^+ (not preadsorbed)) (Figure 5a), the COO^- group is almost anchored to the surface, keeping in close proximity to two adjacent BOH groups. Moreover, the Na^+ ion from the bulk solvent reaches the vicinity of Asp and adsorbs at a TD site, participating in bridging the COO^- group to the surface. The distances from the mediated $\text{Na}^+_{\text{I}-1}$ to the Asp oxygens in system I are calculated to monitor the approaching process of the cation to the residue (shown in Figure 6). At the beginning of the simulation, there is no Na^+ in the vicinity of the Asp (all distances are $>8 \text{ \AA}$). The $\text{Na}^+_{\text{I}-1}$ moves toward the surface and begins to interact directly with the carbonyl oxygen in the C-terminus of RGD ($\text{O}_{\text{CO}-\text{C}}$) at $t = 1.20 \text{ ns}$. From $t = 2.30 \text{ ns}$, the $\text{O}_{\text{CO}-\text{C}}$ moves upward and loses the direct connection with the cation. However, it suddenly approaches the $\text{Na}^+_{\text{I}-1}$ again at $t = 2.50 \text{ ns}$ and drags the cation from position A (Figure 6-(1)) to position B (Figure 6-(2)). Henceforth, the $\text{Na}^+_{\text{I}-1}$ forms bonds with both $\text{O}_{\text{COO}-}$ atoms (shown in Figure 6-(2), (3)). The connections between the $\text{Na}^+_{\text{I}-1}$ and the $\text{O}_{\text{COO}-}$ atoms are

maintained until the end of the simulation, whereas a water molecule is needed to bridge the $\text{O}_{\text{CO}-\text{C}}$ and the $\text{Na}^+_{\text{I}-1}$ (Figure 6-(2)) during $2.50\text{--}5.40 \text{ ns}$. At $t = 5.40 \text{ ns}$, the $\text{O}_{\text{CO}-\text{C}}$ moves closer to the $\text{Na}^+_{\text{I}-1}$ again. Therefore, there are direct bonds between all involved oxygens and the TD $\text{Na}^+_{\text{I}-1}$ (Figure 6-(3)) at the end of the simulation, indicating a strongly bound Asp.

If the COO^- group adopts the initial configuration with one $\text{O}_{\text{COO}-}$ atom H-bonded to the surface and the other not involved in any H bond with the surface (Figure 4b-(1) or 4c-(1)), then the Asp will move into the bulk solvent in the very early stage of the simulation if no preadsorbed Na^+ is presented in the vicinity of the Asp or no Na^+ is able to approach the residue in such a short time (e.g., system II: O_{BO} (near)/ Na^+ (not preadsorbed)). However, if a preadsorbed Na^+ is positioned close to the $\text{O}_{\text{COO}-}$, then the adsorption behavior of Asp will be completely different (e.g., the COO^- group in system III (O_{BO} (near)/ Na^+ (preadsorbed)) remains on the surface during the entire simulation (Figure 4c)). Because one of the $\text{O}_{\text{COO}-}$ atoms in system III is initially close to the O_{BO} without an attached H_{BOH} , the lateral movement or rotation of the COO^- group is the only way to form enough H bonds with the surface. After 4 ns, both $\text{O}_{\text{COO}-}$ atoms can form H bonds with the nearest H_{BOH} (Figure 4c); however, the COO^- group still moves along the [001] direction and rotates a little during the final 2 ns (as indicated in the 2D density map: Figure 5b). The 2D density map of the COO^- group of system III is slightly different from that of system I. The COO^- group in Figure 5b shows a less localized density, indicating multiple positions in the [001] direction (a range from 23.5 to 30 \AA) whereas the COO^- group in Figure 5a remains in the same position (from 20 to 24 \AA). This may partially depend on the stability of the direct bonds between the mediated Na^+ and the $\text{O}_{\text{COO}-}$ atoms, which will be explained below. As shown in Figure 7, the preadsorbed TD $\text{Na}^+_{\text{III}-1}$ (system III) keeps close to both $\text{O}_{\text{COO}-}$ atoms with intermittent separations during the first 1.8 ns. After the arrival of $\text{Na}^+_{\text{III}-2}$ from the bulk solvent (during 1.80 to 3.60 ns), in the vicinity of the $\text{O}_{\text{COO}-1}$, the predominant configuration of COO^- is the one that the $\text{O}_{\text{COO}-1}$ forms direct bonds with two mediated Na^+ ions, whereas the $\text{O}_{\text{COO}-2}$ forms a H bond with the H_{BOH} and a direct bond with the $\text{Na}^+_{\text{III}-1}$ (shown in Figure 7-(1)). The variation of $\text{Na}^+\text{-O}$ distances becomes much smaller during this period, indicating that the approach of two Na^+ decreases the

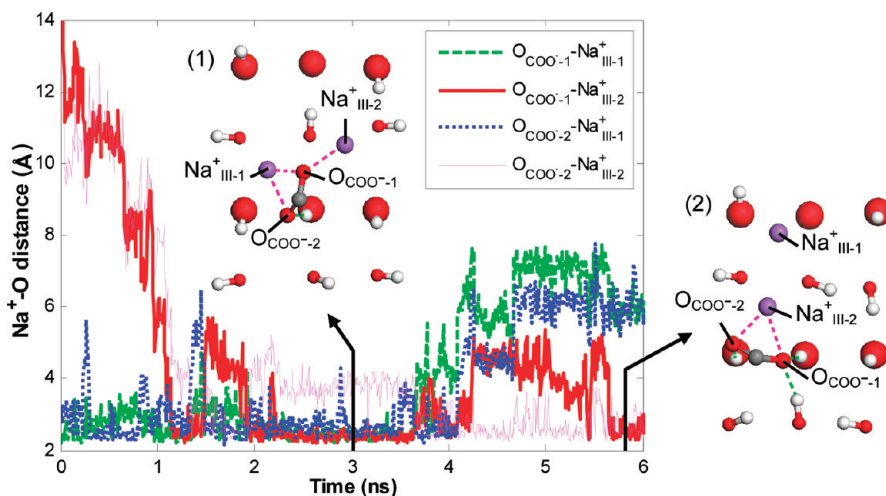


Figure 7. Evolution of the distances from the O_{COO^-} atoms to the specific Na^+ ions in system III during the 6 ns MD production run. In the snapshots, the O_{BOH} and O_{BO} are shown by CPK mode, the H_{BOH} , TOH , COO^- , and the adsorbed Na^+ ions are shown by ball-and-stick mode. The H bonds and direct bonds (between Na^+ and COO^-) are represented by green and magenta dashed lines, respectively.

mobility of the COO^- group. The $\text{Na}^+_{\text{III}-1}$ begins to move away from the COO^- group at $t = 3.60$ ns, leaving the TD $\text{Na}^+_{\text{III}-2}$ to fill the position previously occupied by $\text{Na}^+_{\text{III}-1}$ (Figure 7-(2)); however, the $\text{Na}^+_{\text{III}-2}$ ion is capable of forming direct bonds with both O_{COO^-} atoms only after 5.60 ns. Hence, it is suggested that the Asp side chain cannot be trapped on the binding site solely by the $\text{H}_{\text{BOH}} \cdots \text{O}_{\text{COO}^-}$ H bonds in the absence of stable mediation of Na^+ , which explains the higher mobility of COO^- group in system III than that in system I, where the mediated $\text{Na}_{\text{I}-1}^+$ remains in the close proximity to both O_{COO^-} after 2.5 ns (Figure 6).

To find out the reason for the leaving of $\text{Na}^+_{\text{III}-1}$, we obtained the coordination number of the fully solvated carboxyl oxygen– H_w pair (Figure S5 in the Supporting Information). The mean coordination number of 2.63 indicates that the O_{COO^-} atom has nearly three nearest neighbors. Therefore, it seems reasonable that two mediated Na^+ can approach the free O_{COO^-} (not involved in direct H bonds with the surface), but only one Na^+ is able to form a direct bond with the O_{COO^-} , which is attached to the surface by H bonds. However, when both O_{COO^-} atoms can form enough number of H bonds with the hydroxyls (Figure 7-(2)), the redundant ion leaves for a more favorable adsorption site on the surface. This may result from the coordination saturation of the O_{COO^-} atoms and the high attraction of the negatively charged surface for the cation.

In our simulations, the mediated Na^+ bridges the COO^- group to the surface, enabling the adsorption of Asp side chain to the rutile, even if both are negatively charged. The cation mediation occurs only for the stable TD Na^+ , which is the most popular mode of the adsorbed Na^+ (58.91%, shown in Figure 3). Moreover, this mode is probably the best candidate for cation mediation in the present study because the TD Na^+ makes it possible to maintain adequate number of $\text{Na}^+ \cdots \text{O}_{\text{COO}^-}$ bonds and $\text{H}_{\text{BOH}} \cdots \text{O}_{\text{COO}^-}$ H bonds at the same time, which seems to be favorable for the Asp/ Na^+ /rutile interactions. If the mediated Na^+ adsorbs at a BD-TOTO site when both O_{COO^-} atoms are stably H-bonded to the H_{BOH} , the distances from the Na^+ to the O_{COO^-} atoms may be too long to form $\text{Na}^+ \cdots \text{O}_{\text{COO}^-}$ direct bonds. If the mediated Na^+ adsorbs at a BD-BOTO site, the existence of direct bonds between the Na^+ and both O_{COO^-} atoms seems to

be impossible when the two O_{COO^-} atoms are H-bonded to two adjacent H_{BOH} atoms. This probably applies to the monovalent cations with a similar radius to the Na^+ ; however, the mediation modes of the divalent cations may be different because the charge and the size of ions will largely affect the peptide/ion/rutile interactions. Monti et al.⁵⁸ found that the mediated Ca^{2+} preferred to adsorb between two terminal oxygens on a different negatively charged rutile (110) surface (adding a selected number of TOH groups to the neutral nonhydroxylated surface). The O_{COO^-} atom of the H-Lys-Glu-Lys-NH₂ tripeptide in Monti's simulation detached from its original binding site (a titanium site) and reoriented itself toward the mediated Ca^{2+} ion. This is different from the behavior of COO^- group in our simulations (systems I and III, where both O_{COO^-} atoms keep H-bonded to the binding sites, in coordination with the indirect interactions (mediated by Na^+ ions) with the surface atoms) as a result of the differences in the size and charge of the mediated cations as well as the distributions and types of the hydroxyls on the rutile surfaces. However, the Na^+ ions in the present work and Ca^{2+} ions in Monti's work can compensate for both the carboxyl group and the surface charges, supporting the view that the cations (Na^+ and Ca^{2+}) are actively involved in peptide/surface adsorption, acting as a bridge between the negatively charged COO^- group and the negatively charged rutile surface.

Effect of Na^+ on Arg Desorption. At pH ~ 7.80 , the Arg residue and the rutile surface carry opposite net charges; thus a strong electrostatic attraction is expected between them. However, if the cations are present in the neighborhood of the binding sites, then will this attraction be diminished? When the Asp is far away from the surface, fully solvated by the water, will the Arg remain adsorbed to the surface? The simulations in the present study can shed light on such questions, providing insight into the driving force for Arg staying/leaving in the presence of nearby cations.

The Arg in system III (O_{BO} (near)/ Na^+ (preadsorbed)) stays on the surface for ~ 1.40 ns, and no Na^+ adsorbs stably in its vicinity. The reason for Arg desorption in system III may be attributed to the structural adjustment of the peptide, which will be explained below. The Arg in system I (O_{BO} (far)/ Na^+ (not preadsorbed)) stays on the surface for longer than 2 ns. One Na^+ ion reaches the neighborhood of NH_2 groups and binds to the

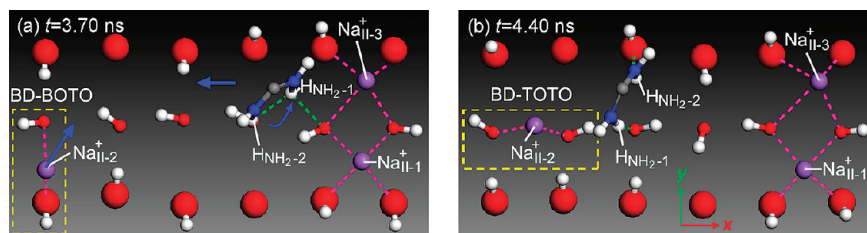


Figure 8. Adsorption conformations of NH_2 groups on the rutile surface in system II. $t =$ (a) 3.70 and (b) 4.40 ns. The bulk TiO_2 is omitted for clarity. O_{BOH} and O_{BO} are shown by CPK mode, and the H_{BOH} , TOH , NH_2 , and the adsorbed Na^+ ions are shown by ball-and-stick mode. The H bonds and direct bonds (connected to the Na^+ ions) are represented by green and magenta dashed lines, respectively. The blue arrows indicate the moving directions of the Na^+ ion and the NH_2 groups.

TOH atom, which originally forms a H bond with the NH_2 -1 group (Figure 4a-(1)). The Arg is pushed to move away from the initial adsorption site and finally leaves the surface at $t = 2.30$ ns. To visualize the Na^+ repulsion to the Arg side chain, we show the configurations of NH_2 groups in system II (O_{BO} (near)/ Na^+ (not preadsorbed)) with three nearby Na^+ ions ($\text{Na}_{\text{II}-1}$, $\text{Na}_{\text{II}-2}$, and $\text{Na}_{\text{II}-3}$) in Figure 8. At $t = 3.70$ ns, the $\text{Na}_{\text{II}-1}$ and $\text{Na}_{\text{II}-3}$ adsorbing at a TD site are much closer to the NH_2 groups than the $\text{Na}_{\text{II}-2}$ occupying a BD-BOTO site (Figure 8a). As indicated by the arrows, the NH_2 groups rotate anticlockwise and move along the $-x$ direction. At $t = 4.40$ ns, the NH_2 groups are farther from the two TD Na^+ ions, whereas the $\text{Na}_{\text{II}-2}$ leaves the BD-BOTO site and adsorbs at a BD-TOTO site close to the NH_2 -1 group (Figure 8b). These movements suggest that the Arg side chain is experiencing interference, in its adsorption with rutile, from three neighboring Na^+ at the same time. To investigate this interference further, the sum of the electrostatic repulsions between the Arg hydrogens (H_{NH_2-1} and H_{NH_2-2} in Figure 8) and the three Na^+ ions ($\text{Na}_{\text{II}-1}$, $\text{Na}_{\text{II}-2}$ and $\text{Na}_{\text{II}-3}$) are calculated according to Coulomb's law. Figure 9 shows the evolution of the NH_2-Na^+ repulsion with simulation time as well as the number of H bonds connecting the Arg hydrogens to the surface oxygens (O_{TOH} , O_{BOH} , and O_{BO}). At the beginning of the simulation, the electrostatic repulsion is lower than 0.50 nN due to large separations between the Arg hydrogens and the three Na^+ ions. As the Na^+ ions move toward the Arg-surface binding site, the repulsion steadily increases and reaches a critical level (nearly 2 nN) at $t = 3.20$ to 3.80 ns (Figure 9a), when the NH_2 groups form two to three H bonds with the surface (Figure 9b). The Arg sporadically rotates and hops along the [001] direction to minimize the electrostatic repulsion from the Na^+ ions, which decreases to 1.13 nN when the NH_2 groups locate near the geometrical center of the three Na^+ (around $t = 4$ ns). The inset in Figure 9a shows the NH_2-Na^+ repulsion and the number of NH_2 -surface H bonds during 4.55 to 4.65 ns. The repulsion again reaches 2.00 nN at $t = 4.60$ ns when the NH_2 groups begin to move into the bulk solvent to relieve this strong repulsion (decreases toward 0 nN), and thus the NH_2 -surface H bonds break ($n_{\text{HB}} = 0$). Therefore, it may be inferred that the Arg is trying to balance the electrostatic repulsion from the neighboring cations and the interaction with the surface by rotation and lateral mobility. However, the Arg is finally driven away from the surface by the approach of three Na^+ ions in both sides to relieve the strong NH_2-Na^+ electrostatic repulsion.

Effect of Conformational Adjustment on RGD Adsorption. RGD is a short peptide without a long flexible backbone, and thus any conformational adjustment may cause the loss of the "horseshoe" configuration. That is, the competition between the Arg

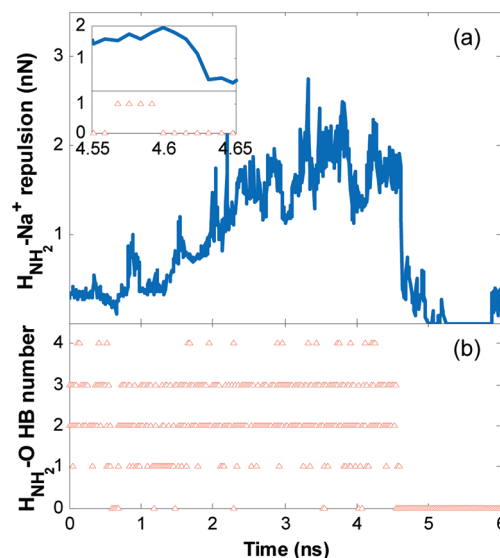


Figure 9. (a) Evolution of the electrostatic repulsion between the hydrogens in NH_2 groups (H_{NH_2-1} and H_{NH_2-2}) and the specific Na^+ ($\text{Na}_{\text{II}-1}$, $\text{Na}_{\text{II}-2}$, and $\text{Na}_{\text{II}-3}$) in system II during the 6 ns MD production run. (b) Evolution of the H-bond number between the hydrogens in NH_2 groups (H_{NH_2-1} and H_{NH_2-2}) and the oxygens on the surface (H_{TOH} , H_{BOH} , and O_{BO}) in system II during the 6 ns MD production run. The inset shows the evolution of the above two items during 4.55 to 4.65 ns.

and the Asp may drive the more weakly attached group away from the surface to meet the structural adjustment. Hence, it is necessary to investigate how the conformational change facilitates the Asp adsorption/Arg desorption. The Arg in system II (O_{BO} (near)/ Na^+ (not preadsorbed)) remains on the surface for 4.60 ns, whereas the Asp moves into the bulk solvent soon after the production run begins. This loss of binding of Asp to rutile may be attributed to the competition with the more strongly attached NH_2 groups, when no mediated Na^+ is available to bridge the O_{COO^-} atoms to the surface. The "horseshoe" configuration is preserved for 2.30 and 1.40 ns in system I (O_{BO} (far)/ Na^+ (not preadsorbed)) and system III (O_{BO} (near)/ Na^+ (preadsorbed)), respectively. To see the movement of RGD along the direction perpendicular to the surface plane, we define the z -component of the vector from the α -carbon (C_α) of Arg to the C_α of Asp ($z\text{-vec}$) in Figure 10a. A value of zero indicates a flat conformation of RGD with Arg C_α and Asp C_α being on the same vertical level. A larger negative value shows that the Arg residue is far away from the binding sites. The angle θ in Figure 10a characterizes the rotational state of RGD in the

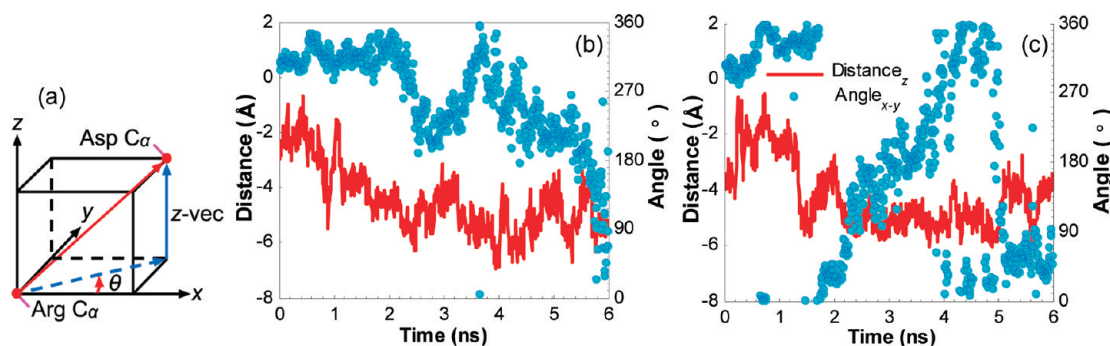


Figure 10. (a) Geometric schemes of *z*-component of the Arg C_α-Asp C_α vector and the rotation angle θ in the *x*-*y* plane. (b) Evolution of *z*-component of the Arg C_α-Asp C_α vector and the rotation angle θ in the *x*-*y* plane for system I. (c) Evolution of *z*-component of the Arg C_α-Asp C_α vector and the rotation angle θ in the *x*-*y* plane for system III.

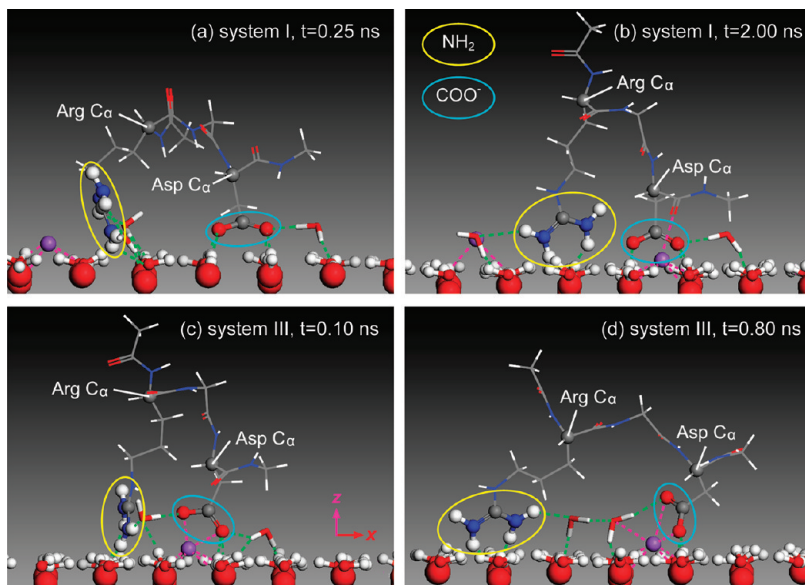


Figure 11. Adsorption conformations of RGD onto the rutile surface. (a) system I: $t = 0.25$ ns, (b) system I: $t = 2.00$ ns, (c) system III: $t = 0.10$ ns, and (d) system III: $t = 0.80$ ns. The bulk TiO₂ is omitted for clarity. The O_{BOH} and O_{BO} are shown by CPK mode, the H_{BOH}, TOH, NH₂, COO⁻, Arg C_α, Asp C_α, and the adsorbed Na⁺ ions are shown by ball-and-stick mode, the rest of the peptide is shown by line mode, and the involved water molecules are shown by stick mode. The H bonds and direct bonds (connected to the Na⁺ ions) are represented by green and magenta dashed lines, respectively. The NH₂ groups and the COO⁻ group are labeled by yellow and cyan circles, respectively.

x-*y* plane. A value of 0° refers to the state where the peptide is located above a rail composed of TOH or BOH (including O_{BO}), and a value of 90° means that RGD is sitting across the rails.

Figure 10b,c shows the evolution of *z*-vec and angle θ for systems I and III, respectively, and Figure 11 gives the representative snapshots of the molecular assemblies (system I: (a),(b); system III: (c),(d)). In Figure 10b, the angle θ fluctuates around 316° during the first 2.30 ns, whereas the *z*-vec decreases steadily, indicating that the peptide is pulled upward gradually from a “lying down” configuration (Figure 11a) into a “standing up” configuration (Figure 11b). After 2.30 ns, the Arg-surface H bonds break and the *z*-vec fluctuates widely. Meanwhile, the dramatic change in the evolution of angle θ suggests a flexible Arg side chain rotating freely in the solvent phase. It should be considered that conformational changes of the peptide are also important, in coordination with rotational dynamics. The Gly Ψ (N-C_α-C-N) and Gly Φ (C-N-C_α-C) backbone dihedrals, which are in the center of the peptide, should dictate these

conformational changes and are shown in Figure S6 in the Supporting Information. In system I, both Gly dihedrals vary slightly in the early production stage, but a sudden decrease from ~60° to nearly -60° in the Gly Ψ and a sharp increase from ~70° to ~180° in the Gly Φ are presented in the dihedral evolution at around $t = 2.30$ ns, which is exactly the same time as the Arg comes off the surface (Figure 4a). That is, the sudden change in the dihedrals at $t = 2.30$ ns causes a marked structural adjustment, which should contribute to the departure of Arg. The step transitions in the Gly dihedrals after 2.30 ns correspond to the peaks in the N_{NH₂}-O_{TOH} distances (Figure 4a), which indicates that the free motion of the Arg after desorption results in conformational adjustment of the peptide.

In system III, both the Arg and the Asp side chains stretch straight to reach the surface during the first 0.20 ns (Figure 11c), resulting in a much lower relative position of Asp C_α due to its shorter side chain (distance_{*z*} = -3.60 Å, Figure 10c). The NH₂ groups gradually move along the [001] direction during 0.20 to

1.40 ns, pulling the “standing up” RGD (Figure 11c) into a “lying down” configuration (Figure 11d) with the maximum of z-vec close to zero. The dramatic change of z-vec during 1.40 to 2.40 ns (Figure 10c) arises from the sudden “leave-return-leave” motion of Arg (Figure 4c). After 2.40 ns, the Arg leaves the surface completely, enabling free rotation, as indicated by the rotation angle spanning almost from 0 to 360°. The Gly dihedrals (Figure S6 (b) in the Supporting Information) increase steadily during the first 1.40 ns, inducing a gradual change of the RGD conformation, which helps to drive the Arg away from the surface. The Gly Ψ decreases from ~80° to around -40° during 1.40 to 2.40 ns, whereas the Gly Φ increases rapidly from -180 to -60° during 2 to 2.40 ns. The dihedrals tend to stabilize when the Arg is fully solvated in the water (after $t = 2.40$ ns). The RGD finally undergoes the “hinge-bending” motion (Figure 4c-(3)) with nearly fixed Gly dihedrals. Therefore, it may be inferred that the conformational adjustment of RGD in coordination with Na⁺ repulsion drives the more weakly attached Arg to leave the surface but holds the more strongly attached Asp on the surface. Conversely, the desorption of Arg allows the conformation to be free during the stage of “hinge-bending” motion.

Perspective of Cation Mediation. Although the involved rutile surface presents a charge density of -0.208 C/m² (pH ~7.80), the negatively charged Asp residue in systems I and III can adsorb on the surface in the NaCl aqueous solution during the entire simulation. This agrees with *in situ* ATR-IR spectroscopy results⁴³ that the Asp residues in solutions containing KCl could bind to the negatively charged rutile surface even at pH 7.5. The presence of Na⁺ can dramatically affect the RGD-rutile binding mode because a different mechanism of binding is available to the Asp and the adsorption of Arg is hindered by the approach of cations. As stated in the Introduction, experimental data showed that the negative charge of TiO₂ surface was screened by cations, and the salt concentration would impact on the protein adsorption.^{30–35} There are two major factors influencing surface charge and adsorption of ions on the metal oxide surfaces: pH (i.e., concentration of H₃O⁺ ions) and salt concentration.^{59,60} Higher pH will result in more negative surface charge and, as a result, in higher surface concentration of compensating cations. In addition, higher salt concentration and therefore cation activity results in higher surface concentration of compensating cations due to their increased competition with the surface protons. The degree of exchange between the surface protons and the cations strongly depends on the type of the cation and on the salt concentration. This effect is strongest at low bulk salt concentrations and becomes negligible at higher concentrations (e.g., ~0.5M) at which the surface is saturated with cations.

It would also be very interesting to compare the screening effect of various cations carrying different amounts of positive charges. Will the screening be more efficient for the divalent cations than the monovalent cations? Will the connection between the negatively charged residue and the negatively charged surface be further strengthened through the mediation of divalent cations? The amount of the adsorbed divalent cations on the negatively charged surface with a specific charge density will be almost half the amount of the adsorbed monovalent cations. Therefore, it is possible that Arg may remain on the surface because the chance of it getting close to a divalent cation is reduced by one-half compared with a monovalent cation; even if the cation approaches the Arg the residue may move to another site on the surface without desorption. This is because the available area of the rutile/water interface, not occupied by the cations, is much larger in the solution containing divalent cations than the one in NaCl solution.

CONCLUSIONS

A single RGD sequence with a “horseshoe” configuration was put close to the negatively charged hydroxylated rutile (110) surface, with special attention to the effect of adsorbed compensating Na⁺ ions on the binding propensities of the charged side chains. The simulation results suggest that the competition between the positively charged Arg side chain and the negatively charged Asp side chains may drive the more weakly attached group away from the surface. O_{TOH} on the surface shows a stronger attraction for the positively charged species (H_w, Na⁺, and NH₂ group) than the O_{BOH}, whereas the H_{BOH} is more attracted to the negatively charged species (O_w and COO⁻ group) than the H_{TOH}. The NH₂ groups exhibit some rotational freedom and lateral mobility along the [001] direction. However, the approach of Na⁺, competing for the adsorption site with the NH₂ groups, combined with the structural adjustment of the peptide drives the Arg residue to detach from the rutile surface. On the contrary, the Na⁺ adsorbed at a TD site in close proximity to the Asp side chain seems to assist in stabilizing the COO⁻ group on the surface and guide it to orientate toward the surface hydroxyls. However, once both O_{COO-} atoms successfully form enough H bonds with the hydroxyls, the redundant ions will leave for a more favorable adsorption site.

The Article provides evidence that the presence of ions is a major factor in determining the adsorption mode of proteins on the metal and metal oxide materials, thus impacting the ultimate biocompatibility of the surface. Controlling the ionic strength or ionic species in the protein precoating stage seems to be feasible to manipulate the binding and release of biomolecules to the implant surface, which is critical for the development of intelligent implant materials. We anticipate that the findings presented here will ultimately contribute to the biomimetic modification of implants, by suggesting how to modify the surface of implants to induce the desirable biological function.

ASSOCIATED CONTENT

S Supporting Information. Available binding modes of a single hydroxyl group with the H-bonded water and the percentage of each mode (per hydroxyl), the geometric scheme of the region occupied by RGD, RDF of fully solvated Na⁺-O_w, the distances from N_{NH₂} to the nearest O_{TOH}, O_{BOH}, and O_{BO}, the distances from O_{COO-} to the nearest H_{TOH} and H_{BOH}, RDF and coordination number of fully solvated carboxyl oxygen-H_w pair, and the evolution of Gly dihedrals for RGD. This material is available free of charge via the Internet at <http://pubs.acs.org>.

AUTHOR INFORMATION

Corresponding Author

*Fax: (615)-3437951. E-mail: wuchunya1982@163.com.

Present Addresses

[†]University of Dayton

ACKNOWLEDGMENT

This work was supported by the Research Fund for the Doctoral Program of Higher Education of China (no. 2010-2302110006). This research used resources of the National Energy Research Scientific Computing Center, which is supported by the Office of Science of the U.S. Department of Energy under Contract no. DE-AC02-05CH11231.

■ REFERENCES

- (1) Gray, J. J. *Curr. Opin. Struct. Biol.* **2004**, *14*, 110–114.
- (2) Andrade, J. D.; Hlady, V. *Adv. Polym. Sci.* **1986**, *79*, 1–63.
- (3) Walker, R. K.; Krishnaswamy, S. *J. Biol. Chem.* **1994**, *269*, 27441–27450.
- (4) Castner, D. G.; Ratner, B. D. *Surf. Sci.* **2002**, *500*, 28–60.
- (5) Hlady, V.; Buijs, J. *Curr. Opin. Biotechnol.* **1996**, *7*, 72–77.
- (6) Tsai, W. B.; Grunkemeier, J. M.; McFarland, C. D.; Horbett, T. A. *J. Biomed. Mater. Res.* **2002**, *60*, 348–359.
- (7) Latour, R. A. *Biointerphases* **2008**, *3*, FC2–FC12.
- (8) Latour, R. A. Biomaterials: Protein-Surface Interactions. In *The Encyclopedia of Biomaterials and Biomedical Engineering*; Informa Healthcare: London, 2008.
- (9) Sarikaya, M.; Tamerler, C.; Jen, A. K. Y. *Nat. Mater.* **2003**, *2*, 577–585.
- (10) Tamerler, C.; Khatayevich, D.; Gungormus, M. *Biopolymers* **2010**, *94*, 78–94.
- (11) Jung, S. Y.; Lim, S. M.; Albertorio, F.; Kim, G.; Garau, M. C.; Yang, R. D. *J. Am. Chem. Soc.* **2003**, *125*, 12782–12786.
- (12) Vroman, L.; Adams, A. L. *J. Colloid Interface Sci.* **1986**, *111*, 391–402.
- (13) Dee, K. C.; Puleo, D. A.; Bizios, R. *An Introduction To Tissue-Biomaterial Interactions*; John Wiley & Sons: Hoboken, NJ, 2003.
- (14) Skelton, A. A.; Liang, T.; Walsh, T. R. *ACS Appl. Mater. Interfaces* **2009**, *1*, 1482–1491.
- (15) Kang, Y.; Li, X.; Tu, Y. Q.; Wang, Q.; Ågren, H. *J. Phys. Chem. C* **2010**, *114*, 14496–14502.
- (16) González-García, C.; Sousa, S. R.; Moratal, D.; Rico, P.; Salmerón-Sánchez, M. *Colloids Surf., B* **2010**, *77*, 181–190.
- (17) Yin, G.; Liu, Z.; Zhan, J.; Ding, F. X.; Yuan, N. *J. Chem. Eng. J.* **2002**, *87*, 181–186.
- (18) Sousa, S. R.; Moradas-Ferreira, P.; Barbosa, M. A. *J. Mater. Sci.: Mater. Med.* **2005**, *16*, 1173–1178.
- (19) Lüthen, F.; Lange, R.; Becker, P.; Rychly, J.; Beck, U. *Biomaterials* **2005**, *26*, 2423–2440.
- (20) Horinek, D.; Serr, A.; Geisler, M.; Pirzer, T.; Slotta, U.; Lud, S. Q. *Proc. Natl. Acad. Sci. U.S.A.* **2008**, *105*, 2842–2847.
- (21) Chen, M. J.; Wu, C. Y.; Song, D. P.; Li, K. *Phys. Chem. Chem. Phys.* **2010**, *12*, 406–415.
- (22) Chen, M. J.; Wu, C. Y.; Song, D. P.; Dong, W. M.; Li, K. *J. Mater. Sci.: Mater. Med.* **2009**, *20*, 1931–1938.
- (23) Forte, G.; Grassi, A.; Marletta, G. *J. Phys. Chem. B* **2007**, *111*, 11237–11242.
- (24) Zhang, H. P.; Lu, X.; Leng, Y.; Watari, F.; Weng, J.; Feng, B.; Qu, S. X. *J. Biomed. Mater. Res., Part A* **2011**, *96*, 466–476.
- (25) Brighton, C. T.; Albelda, S. M. *J. Orthop. Res.* **1992**, *10*, 766–773.
- (26) Grzesik, W. J.; Robey, P. G. *J. Bone Miner. Res.* **1994**, *9*, 487–496.
- (27) Rammelta, S.; Illert, T.; Bierbaum, S.; Scharnweber, D.; Zwipp, H.; Schneiders, W. *Biomaterials* **2006**, *27*, 5561–5571.
- (28) Ferris, D. M.; Moodie, G. D.; Dimond, P. M.; Gioranni, C. W. D.; Ehrlich, M. G.; Valentini, R. F. *Biomaterials* **1999**, *20*, 2323–2331.
- (29) Schneider, J.; Ciacchi, L. C. *J. Chem. Theory Comput.* **2011**, *7*, 473–484.
- (30) Topoglidis, E.; Campbell, C. J.; Cass, A. E. G.; Durrant, J. R. *Langmuir* **2001**, *17*, 7899–7906.
- (31) Jonsson, C. M.; Jonsson, C. L.; Estrada, C.; Sverjensky, D. A.; Cleaves, H. J.; Hazen, R. M. *Geochim. Cosmochim. Acta* **2010**, *74*, 2356–2367.
- (32) Jonsson, C. M.; Jonsson, C. L.; Sverjensky, D. A.; Cleaves, H. J. *Langmuir* **2009**, *25*, 12127–12135.
- (33) Sano, K. I.; Shiba, K. *J. Am. Chem. Soc.* **2003**, *125*, 14234–14235.
- (34) Hayashi, T.; Sano, K. I.; Shiba, K.; Kumashiro, Y.; Iwahori, K.; Yamashita, I. *Nano Lett.* **2006**, *6*, 515–519.
- (35) Hayashi, T.; Sano, K. I.; Shiba, K.; Iwahori, K.; Yamashita, I.; Hara, M. *Langmuir* **2009**, *25*, 10901–10906.
- (36) Ridley, M. K.; Machesky, M. L.; Palmer, D. A.; Wesolowski, D. *Colloids Surf., A* **2002**, *204*, 295–308.
- (37) Předota, M.; Bandura, A. V.; Cummings, P. T.; Kubicki, J. D.; Wesolowski, D. J.; Chialvo, A. A. *J. Phys. Chem. B* **2004**, *108*, 12049–12060.
- (38) Roddick-Lanzilotta, A. D.; McQuillan, A. J. *J. Colloid Interface Sci.* **1999**, *217*, 194–202.
- (39) Roddick-Lanzilotta, A. D.; Connor, P. A.; McQuillan, A. J. *Langmuir* **1998**, *14*, 6479–6484.
- (40) Okazaki, S.; Aoki, T.; Tani, K. *Bull. Chem. Soc. Jpn.* **1981**, *54*, 1595–1599.
- (41) Parikh, S. J.; Kubicki, J. D.; Jonsson, C. M.; Jonsson, C. L.; Hazen, R. M.; Sverjensky, D. A. *Langmuir* **2011**, *27*, 1778–1787.
- (42) Sverjensky, D. A.; Jonsson, C. M.; Jonsson, C. L.; Cleaves, H. J.; Hazen, R. M. *Environ. Sci. Technol.* **2008**, *42*, 6034–6039.
- (43) Roddick-Lanzilotta, A. D.; McQuillan, A. J. *J. Colloid Interface Sci.* **2000**, *227*, 48–54.
- (44) Předota, M.; Vlček, L. *J. Phys. Chem. B* **2007**, *111*, 1245–1247.
- (45) LAMMPS Molecular Dynamics Simulator <http://lammps.sandia.gov> (accessed Jan 18, 2011).
- (46) Cornell, W. D.; Cieplak, P.; Bayly, C. I. *J. Am. Chem. Soc.* **1995**, *117*, 5179–5197.
- (47) Bandura, A. V.; Kubicki, J. *J. Phys. Chem. B* **2003**, *107*, 11072–11081.
- (48) Skelton, A. A.; Walsh, T. R. *Mol. Simul.* **2007**, *33*, 379–389.
- (49) Hoover, W. G. *Phys. Rev. A* **1985**, *31*, 1695–1701.
- (50) Wu, C. Y.; Chen, M. J.; Guo, C. Q.; Zhao, X.; Yuan, C. S. *J. Phys. Chem. B* **2010**, *114*, 4692–4701.
- (51) Köppen, S.; Lang, W. *Surf. Sci.* **2006**, *600*, 2040–2050.
- (52) Gilli, G.; Gilli, P. *J. Mol. Struct.* **2000**, *552*, 1–15.
- (53) García, A. E.; Stiller, L. *J. Comput. Chem.* **1993**, *14*, 1396–1406.
- (54) Obst, S.; Bradaczek, H. *J. Phys. Chem.* **1996**, *100*, 15677–15687.
- (55) Song, D. P.; Chen, M. J.; Liang, Y. C.; Bai, Q. S. *Acta Biomater.* **2010**, *6*, 684–694.
- (56) Předota, M.; Zhang, Z.; Fenter, P.; Wesolowski, D. J.; Cummings, P. T. *J. Phys. Chem. B* **2004**, *108*, 12061–12072.
- (57) Carravetta, V.; Monti, S. *J. Phys. Chem. B* **2006**, *110*, 6160–6169.
- (58) Monti, S.; Alderighi, M.; Duce, C.; Solaro, R.; Tiné, M. R. *J. Phys. Chem. C* **2009**, *113*, 2433–2442.
- (59) Dove, P. M.; Craven, C. M. *Geochim. Cosmochim. Acta* **2005**, *69*, 4963–4970.
- (60) Machesky, M. L.; Wesolowski, D. J.; Rosenqvist, J.; Předota, M.; Vlček, L.; Ridley, M.; Kohli, V.; Zhang, Z.; Fenter, P.; Cummings, P. T. *Langmuir* **2011**, *27*, 4585–4593.

■ NOTE ADDED AFTER ASAP PUBLICATION

This manuscript was originally published on the web on October 25, 2011, with errors to the Introduction and Simulation Methodology Section. The corrected version was reposted with the issue on November 10, 2011.